The International Journal of Advanced Manufacturing Technology (2018) 95:4117–4128
https://doi.org/10.1007/s00170-017-1505-5

ORIGINAL ARTICLE

Friction welding of AA6061 to AISI 316L steel: characteristic analysis and novel design equipment

Long Wan[1] · Yongxian Huang[1]

Received: 19 June 2017 / Accepted: 17 December 2017 / Published online: 5 January 2018

Abstract
AA6061 aluminum alloy and AISI 316L steel were joined by friction welding with a specific steel collar fixed on aluminum side to control its expelling, flash morphology, and the formation of intermetallic compound (IMC) layer. The effects of friction time and welding groove were investigated by analyzing microstructure characteristics and mechanical properties. Eight typical zones could be found, and the existence of some certain zones depended on friction time. The thickness of IMC layers declined from 4 to 0.2 μm with friction time decreasing from 40 to 10 s, while a 15° welding groove machined on the end of steel helped realize thinning of IMC layer to a thickness of 0.3 μm. The conditions of 25-s friction time and processing of the 15° welding groove got best mechanical properties with average tensile strength of 166.32 MPa and average elongation rate of 9.47%. Tensile strength and elongation rate can improve 16.15 and 745.5%.

Keywords Friction welding · Aluminum alloy · Steel · Mechanical property · Interfacial microstructure · Novel design equipment

1 Introduction

With the prompt evolution of modern industries like aerospace, automobile, and shipbuilding, energy savings and cost reduction become inevitable issues encountered. Hybrid structures of aluminum alloy and steel therefore have attracted rising attention for felicitously combining fine mechanical properties of the steel with low-density, high specific strength, and good corrosion resistance of aluminum alloy, which helps reduce fuel consumption by weight saving. Research conducted on welding of aluminum alloy to steel ranges from fusion to solid-state welding processes [1–3]. Each method applies to certain circumstances, but also subjects to some restrictions. Arc brazing [4, 5] and laser brazing [6–8] are easy to operate, but unavoidable intermetallic compounds (IMCs) at the joint interface weaken ultimate tensile strength; diffusion joints are of high strength but are always restricted by the size of vacuum furnace [9]; resistance spot welding is characterized by high productivity, but its joint shows low strength [10]. Other methods like magnetic pressure seam welding [11], electromagnetic impact welding [12], ultrasonic welding [13], and friction stir welding [14–18] all have been studied. Traditional fusion welding between aluminum alloy and steel is of great difficulty due to their large differences in thermodynamic properties such as melting point and thermal conductivity. The differences bring about non-negligible asynchronous fusion, distortion, and residual stresses [5, 6]. Moreover, low solubility of Fe in Al results in the formation of thick and brittle Al-rich IMCs due to high heat input, leading to the degradation of mechanical properties.

Low heat-input welding processes like friction welding have a mechanical solid-state nature, in which heat generated by friction is used to create high-integrity joints between similar or dissimilar metals [19, 20]. It facilitates joint formation of aluminum alloy and steel combination at relatively lower temperatures with a rapid thermal cycle, thus formation of brittle IMCs is depressed [21]. Besides, oxide films on aluminum alloy surface will be eliminated as a result of sufficient rubbing effect between materials involved; hence, fresh aluminum alloy would be exposed, which enables bonding metals to make a sound contact [22]. Feasibility of friction-welded Al/steel joints has already been confirmed [23, 24], and it should be emphasized that sufficient mechanical properties could be achieved only under optimized conditions. Friction time has a definitive effect on joint performances

✉ Long Wan
wanlong178@163.com

[1] State Key Laboratory of Advanced Welding and Joining, Harbin Institute of Technology, Harbin 150001, People's Republic of China

due to the fact that energy required for joining is obtained by means of friction between materials to be welded. Lee et al. [25] used a brake-type friction welding machine to join 5052 aluminum alloy/A36 steel and studied effects of upsetting pressure and friction time on the joint strength. The thickness of the IMC layers increased with increasing friction time. Fuji [26] investigated how friction pressure, friction time, and post-weld heat treatment influenced the joints of 6061 aluminum alloy to Ni–Cr–Mo low alloy steel and found that joint tensile strength decreased with increasing friction time. In contrast, friction pressure was not found to be a significant factor. In addition, Fukumoto et al. [27] studied friction welding of industrial pure 1050 aluminum, 5052 aluminum alloy, and 6061 aluminum alloy to SUS304 austenitic stainless steel and concluded that joint strength increased with elevated friction time but then declined for prolonged friction time. Despite all the previous researches, effects of friction time exhibited irregularity. Nevertheless, how friction time affects thermodynamics process and, in turn, influences joint performances remains unclear.

As mentioned above, formation of thick and brittle Al-rich IMC layers when joining Al/steel is restrained as heat input is relatively low in friction welding. However, inappropriate processing parameters could boost IMC layers' growth and thus deteriorate joint quality. So, finding ways to control the thickness of IMC layers at the interface is of great significance. Ikeuchi et al. [28] investigated the effects of carbon content of steel on IMC layers' growth and tensile strengths. In addition, Reddy et al. [29] employed Ag interlayers as a diffusion barrier for element Fe to control the presence of continuous Fe_2Al_5 layers when welding AISI 304 to AA6061.

From the available literatures, very scant research has been carried out on the partitioning evaluation of interfacial microstructure, which is absolutely necessary because there are huge differences in mechanical properties and microstructural characteristics among different parts of the joint cross section. Moreover, when axial force is exerted during friction welding, plasticized aluminum alloy tends to be extruded out, leading to unavoidable material waste and affecting bonding, so it is also essential to control extrusion of the material. This study investigates the feasibility of friction welding between AA6061 and AISI 316L. A specific steel collar is clamped onto AA6061 side to control the expelling of aluminum alloy, flash morphology, and the formation of IMC layer. Partitioning evaluation of interfacial microstructure of the joint is carried out to understand the thermodynamics process. The idea of processing welding groove on the steel rod end is proposed, and the effect of welding groove on the controlling of IMC layers is described.

2 Experimental details

Rods of 6061 aluminum alloy and AISI 316L austenitic stainless steel with a diameter of 80 mm were used. They were cut to lengths suitable for installation. Before welding, ends of both rods were lathed and then polished mechanically and chemically. Chemical compositions for these two base metals are given in Table 1.

Figure 1 shows schematic and actual illustrations of the simple setup of the facilities. The welding tests were carried out using a MC-130T friction welding machine, with appropriate clamping, fixtures, and machining settings, as shown in Fig. 1a, b. The welding fixtures with an internal diameter slightly larger than 80 mm are shown in Fig. 1c. During the conventional friction welding process, a large number of aluminum alloy were expelled in the form of flash after being heated by the rubbing effect, as shown in Fig. 1d. This was disadvantageous to atomic bonding between the metals and caused material waste. A novel design equipment with specific steel collar, as presented in Fig. 1c, was developed to control the expelling of plastic deformed aluminum alloy via changing morphology of the flash (shown in Fig. 1e). Besides, the collar, fixed on aluminum alloy side, allows a larger upsetting pressure during the process while retards heat dissipation and, in turn, facilitates a more compact bonding.

During the welding process, AA6061 alloy was rotated, while AISI 316L steel was held and the pressure was exerted through steel rod. The friction welding procedures included three stages: primary friction, secondary friction, and upsetting. The primary friction stage employed relatively lower axial pressure (P1 = 34.2 MPa) to preheat the contact zone. The friction coefficient between the materials declined due to elevated temperature, and the possibility of "drop-dead halt" was depressed. The primary friction time settled at 4 s, while the secondary friction time varied from 4 to 40 s to investigate the effect of heat input on joint quality. Friction pressure in secondary friction stage (P_2) rose to 57 MPa, and aluminum alloy close to the contact zone was plasticized as temperature climbed up. During the upsetting stage, the relative motion between two metals halted; subsequently, pressure (P_3) with a large value of 152 MPa was imposed. Afterwards,

Table 1 Chemical compositions of the base metals (wt%)

Composition	C	Si	Cr	Cu	Mn	Mg	Zn	Ti	S	P	Ni	Mo	Al	Fe
AA6061	–	0.4–0.8	0.04–0.35	0.15–0.40	0.15	0.8–1.2	0.25	0.15	–	–	–	–	Bal.	0.7
AISI 316L	≤0.03	≤1.0	16.0–18.0	–	–	–	–	–	≤0.03	≤0.035	12.0–16.0	2.0–3.0	–	Bal.

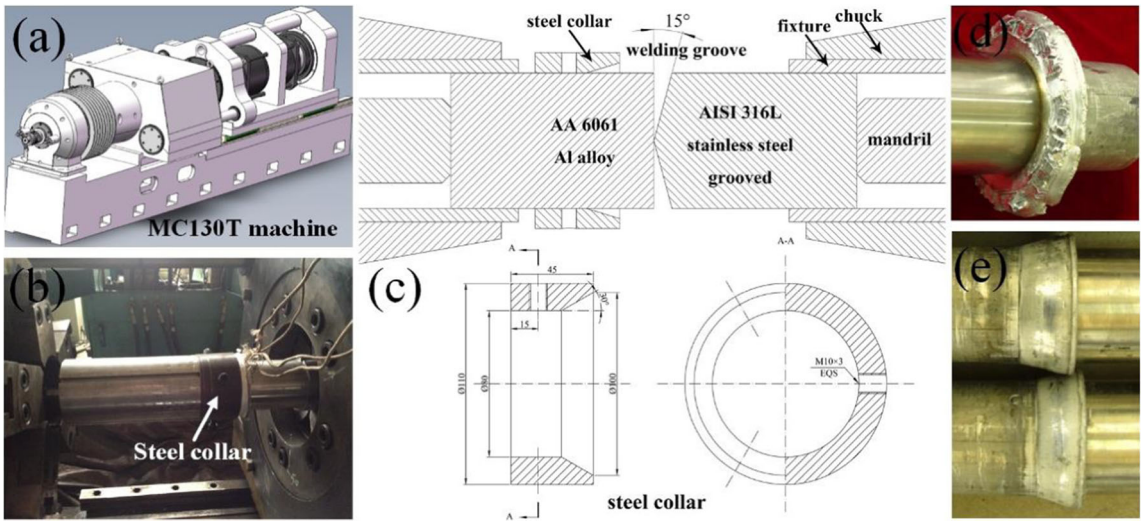

Fig. 1 Schematic and actual illustrations of novel design equipment. **a** Schematic illustration of FS machine. **b** Actual machine. **c** Simple setup of the facilities with specific steel collar (dimensions in mm). **d** Surface formation without specific steel collar. **e** Surface formation with specific steel collar

to verify the practicability of controlling IMC layers via a welding groove, a 15° welding groove was machined on the steel rod end in the fifth experiment, while the aluminum alloy end was kept normal to the end of bar stock for joining. The parameters of all the experiments are given in Table 2.

The transverse weld cross sections were cut by electrical discharge machining and prepared by standard metallographic procedures. The steel side was etched by a solution (2.5 ml nitric acid + 97.5 ml ethanol), while the Al side was etched by Keller's reagent (1 ml HF + 1.5 ml HCl + 2.5 ml HNO_3 + 95 ml H_2O). The microstructure of the joint and element distribution along the interface were observed and analyzed by optical microscopy (OM, Olympus MPG3) and scanning electron microscopy (SEM, Hitachi S-4700) equipped with energy-dispersive spectroscopy (EDS). Microhardness analyses of aluminum alloy side were carried out to get a better understanding of the microstructure variation of aluminum alloy and thermodynamics of the process. The microhardness value of the as-received AA6061 aluminum alloy was 106.8 HV. Microhardness measurements on the weld cross section were carried out employing a HX-1000 Vickers microhardness tester with a load of 500 mgf, for 10 s, to analyze microstructural evolution in the vicinity of weld interface on the aluminum alloy side. Tensile tests were carried out at a loading speed of 1 mm/min by an Instron 5569 electronic universal material testing machine. Specimens of the tensile tests were designed as in Fig. 2. In order to specify the temperature histories of the friction welding joints, temperature distribution was measured through type K thermocouples.

3 Results and discussion

3.1 Macro- and microstructure of the joints

Optical image of AA6061 aluminum alloy microstructure showed relative large grains with the dispersive distribution of acicular Mg_2Si, as presented in Fig. 3a. Microstructural image of the as-received base metal of AISI 316L austenitic stainless steel is shown in Fig. 3b. A few γ-Fe phases were distributing along the rolling direction in the austenite matrix.

Table 2 Parameters for the friction welding experiments

Experiment no.	Rotation speed (N, r min^{-1})	Friction pressure (MPa)		Friction time (s)		Upsetting pressure (P_3, MPa)	Welding groove (θ)
		Primary (P_1)	Secondary (P_2)	Primary (T_1)	Secondary (T_2)		
1	580	34.2	57	4	4	152	0
2	580	34.2	57	4	10	152	0
3	580	34.2	57	4	25	152	0
4	580	34.2	57	4	40	152	0
5	580	34.2	57	4	25	152	15°

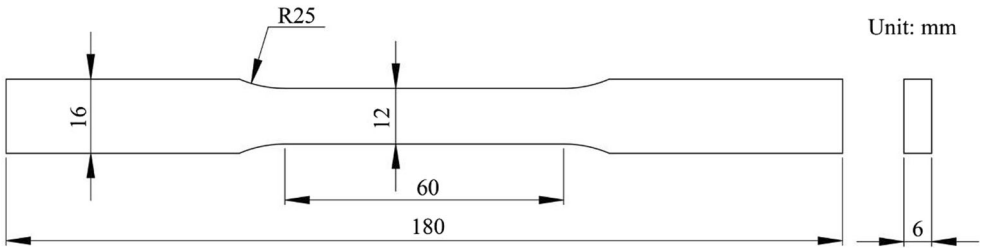

Fig. 2 Dimensions of tensile specimen

With increasing friction time, more heat was generated, leading to the enlargement of the heat-affected zone (HAZ). Thus, specimen employing the longest friction time (T_2 = 40 s) possessed the most comprehensive region characteristics and was supposed to be chosen for partitioning evaluation. Figure 4 shows the division of the joint. On the AISI 316L side, region A refers to base metal (BM), while region B was the heat- and deformation-affected zone (HDZ). In the HDZ, grains were significantly smaller, while the crystal boundaries were broadened due to accumulation of dislocations, as indicated in Fig. 5b.

Since the strength of AISI 316L outstripped that of AA6061 alloy a lot, its microstructural characterization could not definitively affect mechanical properties of the joints. The AA6061 alloy microstructure at and near the weld was complicated. Microstructural features of AA6061 alloy could be divided into regions as follows: region C referred to interfacial zone (IZ) consisted of IMCs. Region D, the solid solution zone, was close to the weld interface in light color (shown in Fig. 5b), illustrating insufficient precipitation of secondary phases due to the fact that this region experienced the highest temperature and fastest cooling rate, and there was not enough time for secondary phases here to precipitate after solution into matrix [30]. Region E referred to partial secondary recrystallization zone. The refined and equiaxed grains caused by recrystallization with few large-sized grains could be clearly observed in Fig. 5c. The nucleation and growth of new grains occurred under the coupling effect of plastic deformation and high temperature. However, the heat input and time were insufficient for further growth and only few grains got to grow up via annexing small grains around, as indicated in Fig. 5c. Region F referred to recrystallization zone consisted of equiaxed grains. New crystal nuclei emerged when temperature was adequate for recovery, and they grew abruptly into equiaxed grains, as shown in Fig. 5d. Region G referred to partial recrystallization zone and was hard to catch a part full of equiaxed grains. Recrystallization was incomplete because temperature in this region was lower than that in recrystallization zone. Region H referred to plastic deformation zone. This region was far from the interface that it was less affected by friction heat, and heat input was inadequate for recrystallization. A bulk of AA6061 alloy experienced plastic deformation and was expelled in the upsetting stage, forming stream morphology along the direction in which they were extruded.

3.2 Effect of friction time and welding groove

Optical microstructure images of specimens 1–4 (T_2 = 4, 10, 25, and 40 s, respectively) are shown in Fig. 6a–d. The image of specimen 1 (T_2 = 4 s) shows that there was only plastic deformation zone (region H) on the aluminum alloy side. The exceedingly short friction time resulted in inadequate temperature for neither solid solution nor recrystallization during upsetting stage. When T_2 reached 10 s, a solid solution zone (region D) in lighter color emerged between the joint interface and the plastic deformation zone (region H). Compared to specimen 1, secondary phases close to the joint interface of specimen 2 dissolved into the aluminum matrix owing to elevated temperature. Afterwards, during the upsetting stage, aluminum alloy at and near the joint interface experienced high cooling rate due to high heat conductivity

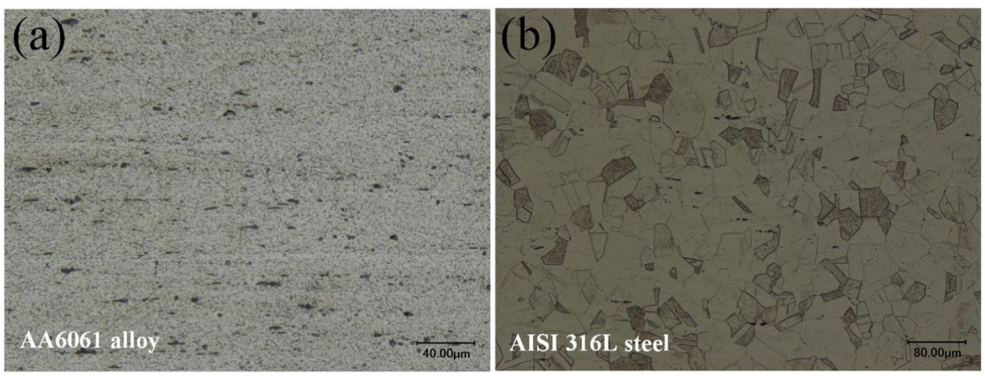

Fig. 3 Microstructural images of as-received base metals of **a** AA6061 aluminum alloy and **b** AISI 316L austenitic stainless steel

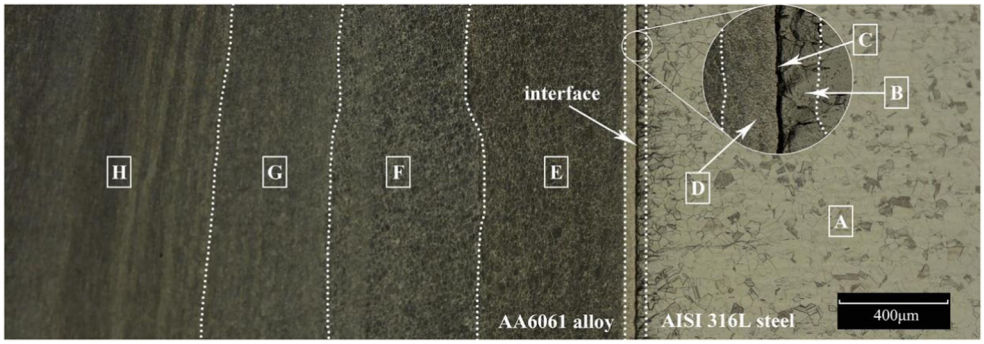

Fig. 4 The division of the joint for partitioning evaluation when friction time (T_2) was 40 s

coefficient; hence, there was not enough time for secondary phases to precipitate, resulting in the emergence of the solid solution zone. When T_2 climbed up to 25 s, width of the solid solution zone (region D) increased to 153.4 μm compared to 27.4 μm of specimen 2. This result suggested that with the increasing of friction time, more heat was conducted to aluminum alloy side and secondary phases got to dissolve into the aluminum matrix from a wider range. Moreover, a partial recrystallization zone (region G) formed due to the high temperature which was enough for recrystallization during the upsetting stage. However, recrystallization in this region exhibited inadequacy, because temperature gradually dropped to a degree under the recrystallization temperature before it was completed. The optical microstructure of specimen 4 (T_2 = 40 s) has been described before. In this case, heat was further conducted to aluminum alloy side and temperature at and near the weld interface climbed up to a degree at which the aluminum alloy could complete the recrystallization, giving rise to the presence of a recrystallization zone near the partial recrystallization zone to the weld interface side. After the completion of the recrystallization, secondary recrystallization happened at the region where the temperature was still higher than the recrystallization temperature, thereby between the recrystallization zone (region F) and the joint interface lied a partial secondary recrystallization zone (region E).

Figure 6e shows the joint microstructure of specimen 5, in which a 15° welding groove was machined on the end of the steel. Compared with specimen 3, specimen 5 had the same typical microstructural partition, which contained IZ, solid solution zone, partial recrystallization zone, and plastic deformation zone. The welding groove has no effects on the relative velocity between the workpieces. The heat input remained the same, and the partition characteristics would not convert too much. However, the difference was that the width of the solid

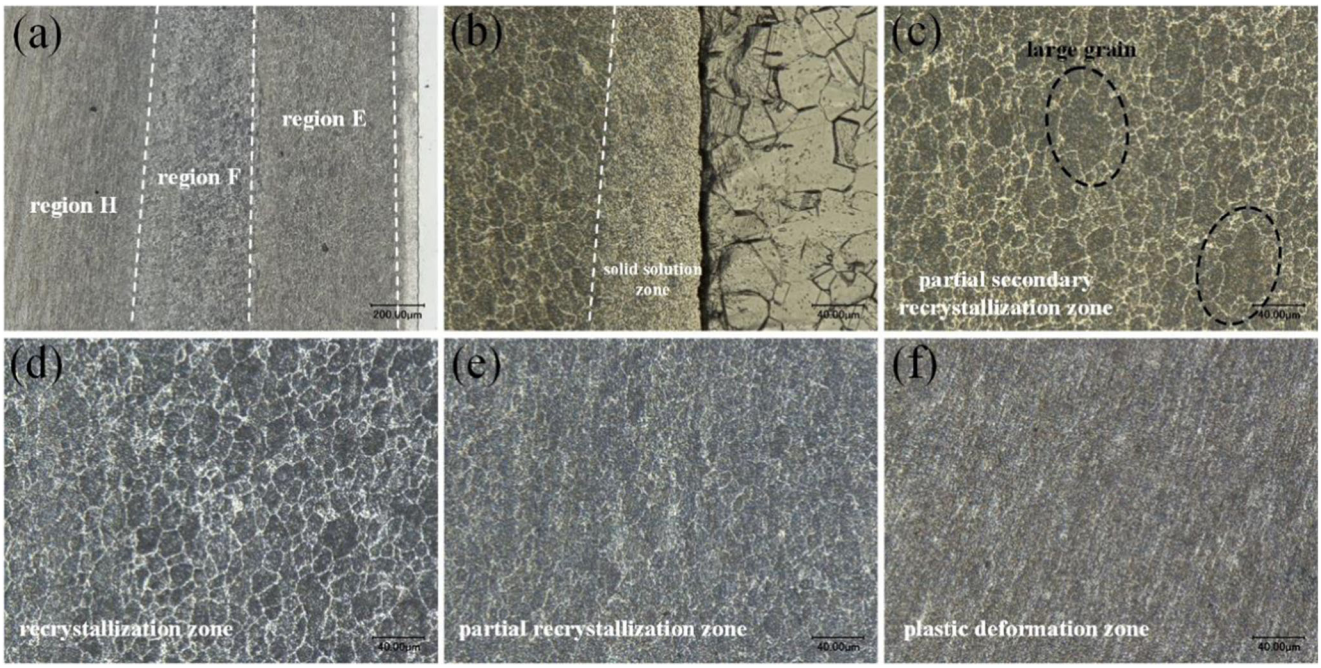

Fig. 5 Microstructure characteristic of typical region shown in Fig. 4. **a** Region (D–H). **b** Region D, the solid solution zone. **c** Region E, the partial secondary recrystallization zone. **d** Region F, the recrystallization zone. **e** Region G, the partial recrystallization zone. **f** Region H, the plastic deformation zone

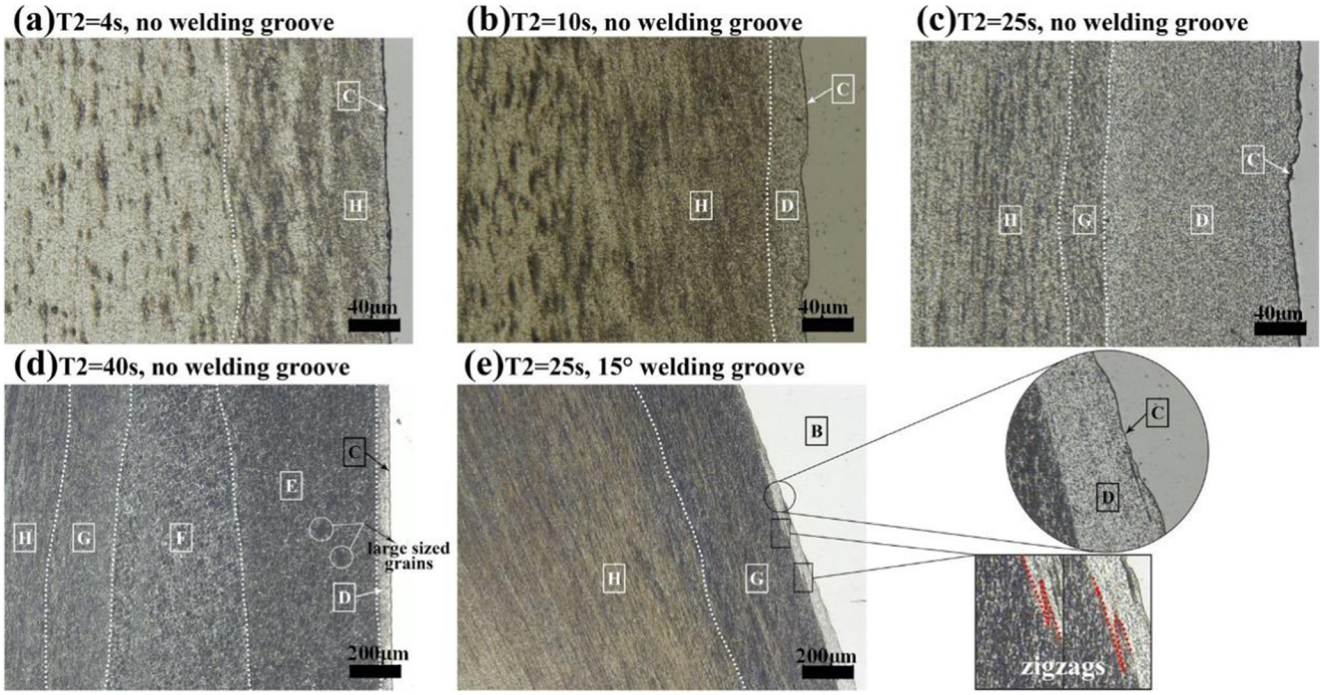

Fig. 6 The effects of friction time and welding groove on the microstructure of the joints. Optical microstructure images of **a** specimen 1, **b** specimen 2, **c** specimen 3, **d** specimen 4, and **e** specimen 5

solution zone in specimen 5 was narrow at the center and broader towards the periphery. This result suggested that processing of welding groove promoted the expelling of plasticized aluminum alloy. In the meanwhile, the appearance of some zigzags on the edge of the solid solution zone coincided with this point.

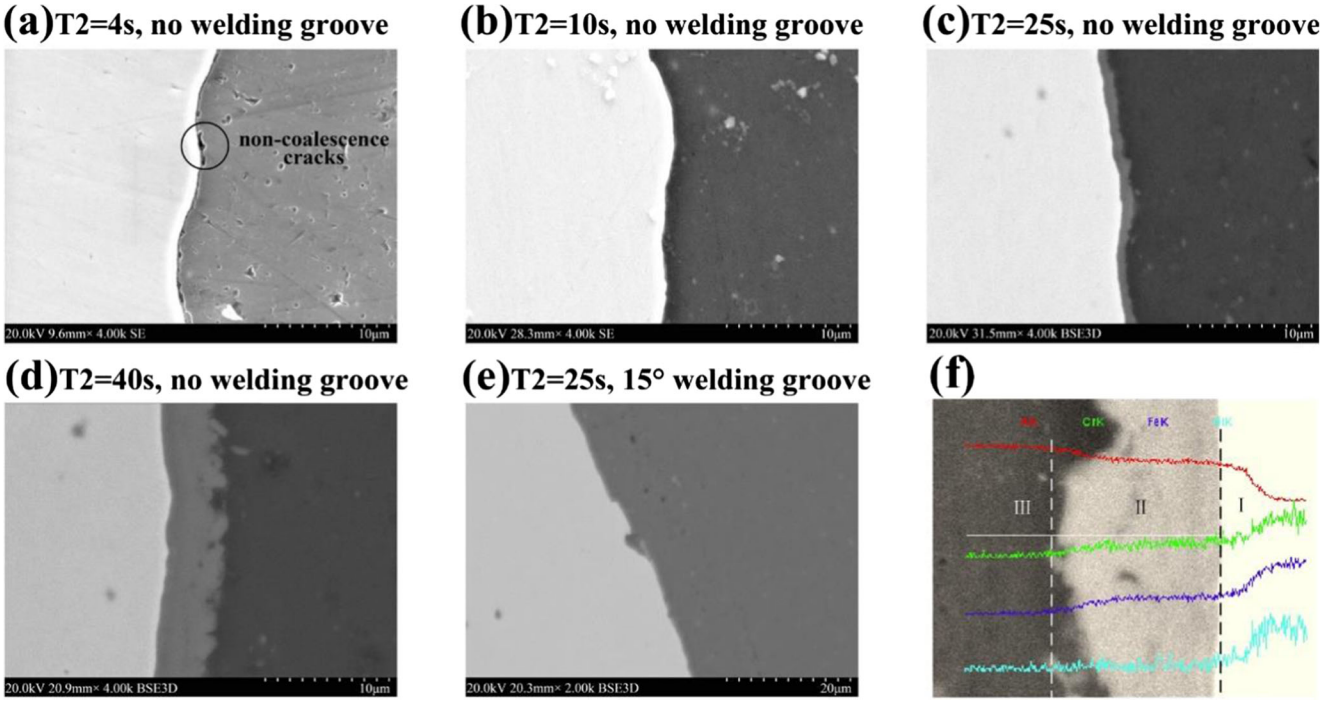

Fig. 7 SEM images of the Al/steel friction-welded joint interface with different welding parameters. **a** Specimen 1. **b** Specimen 2. **c** Specimen 3. **d** Specimen 4. **e** Specimen 5. **f** SEM line scanning result across the interface of the joint

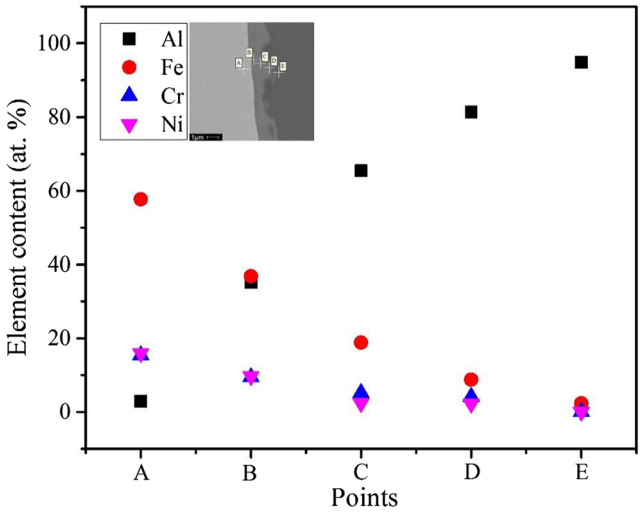

Fig. 8 The EDS analysis results of IMC layer at the interface when the T_2 was 40 s

3.3 Interfacial characteristic of the joint

Short friction time results in low welding temperature, and aluminum alloy could not reach to thermoplastic state, so diffusion between aluminum alloy and steel could hardly occur. In contrast, long friction time brings about high temperature at the joint interface. The aluminum alloy would be weakened and the formation of brittle IMCs would deteriorate the joint strength [31]. SEM observations on specimens 1–4 were performed to obtain information about the thickness and morphology of IMCs at the aluminum alloy/steel joint interface, as presented in Fig. 7a–d. IMC layers could hardly be observed in joint with low heat input ($T_2 = 4$ s); worse still, the reaction between the materials involved was insufficient, causing the presence of non-coalescence cracks. IMC layers with a thickness of 0.2 and 1.0 μm formed at the interface of specimen 2 ($T_2 = 10$ s) and specimen 3 ($T_2 = 25$ s), respectively, while the thickness of IMC layer at the interface of specimen 4 ($T_2 = 40$ s) could exceed 4.0 μm. It was obvious that IMC layers' growth was promoted by increasing friction time. With respect to one single specimen, thickness of the IMC layers increased at the interface from the center to the periphery due to the difference in temperature. The linear velocity at the peripheral part of the interface was comparatively high, and the heat input was larger than that at the central part, causing the thickness variation. SEM line scanning had been done across the transverse section which justified the formation of IMC. A thick and continuous intermetallic layer at the interface apparently grew into the aluminum side of the joint. The presence of other atoms in Al substrate such as Ni and Cr was negligible, as observed from Fig. 7f.

In the sample with $T_2 = 40$ s, shown in Fig. 8, the aluminum matrix was dark, whereas the steel component appeared with a light gray contrast. The interface appeared as a new phase with a halftone lighter contrast. The features of the interface shown that the interface was jagged as it grown into aluminum component. The EDS traces also suggested the existence of the interdiffusion between aluminum and iron atoms, particularly of iron into the aluminum. Similar growth on a smaller scale was also observed in the steel component direction. EDS analysis results confirmed that the joint interface contained some IMCs. Spectra B and C were taken from the intermetallic layer. The compositions of the layer were 35.8 at.% Al, 36.9 at.% Fe, 65.4 at.% Al, and 18.8 at.% Fe with some other minor elements, respectively. This corresponded to a FeAl and $FeAl_3$ intermetallic layer.

In order to control the growth of IMC layers at the interface, this paper developed a method of processing a 15° welding groove on AISI 316L side and studied its influence on the formation of IMC layers. Figure 7e shows the SEM image of specimen 5 (with a 15° welding groove). IMC layer with a thickness of 0.3 μm was observed. Compared with a 1.0-μm-thick IMC layer at the interface of specimen 3, the thickness of IMC layer apparently decreased. The result illustrated that processing of the welding groove on the steel side

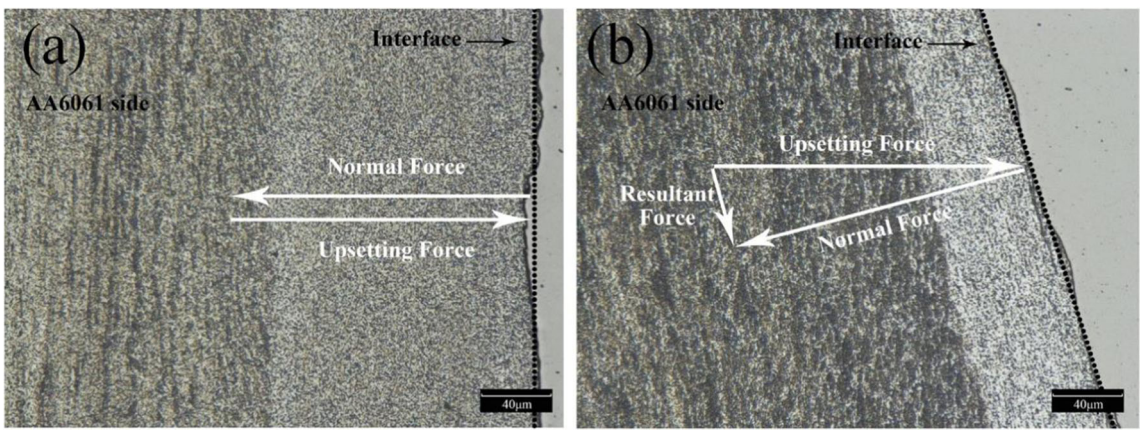

Fig. 9 The comparisons of force analysis of aluminum alloy near the interface. **a** Without welding groove. **b** With a 15° welding groove

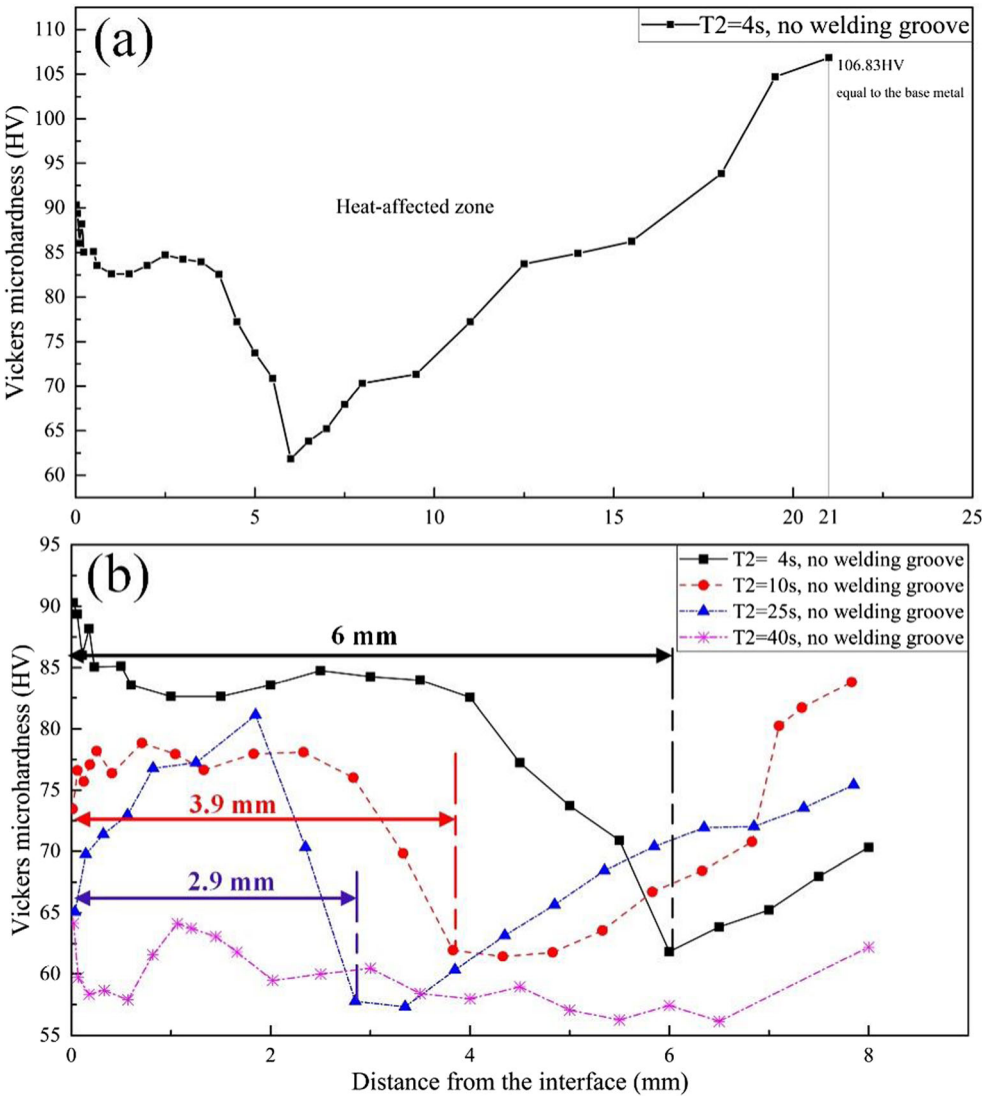

Fig. 10 Microhardness distribution obtained from different specimens. **a** Microhardness distribution of specimen 1 ($T_2 = 4$ s). **b** The comparison of microhardness distributions from a range within an 8-mm distance from the interface on the aluminum alloy side

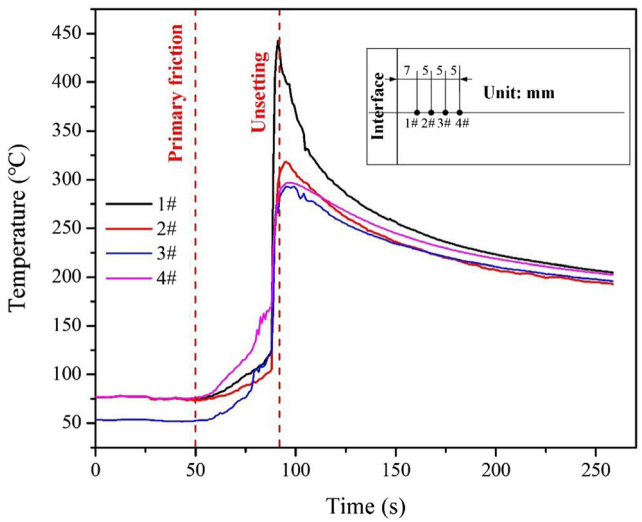

Fig. 11 The results of temperature measurements when T_2 was 40 s. The inserted picture shows the temperature measurement points in the workpiece

could help control the formation of the IMCs to a certain degree. The reason for this could be explained with force analysis on the aluminum alloy side in the vicinity of joint interface. The huge upsetting force would be imposed on the workpieces during upsetting stage; however, load conditions of aluminum alloy near the interface with or without welding groove were different, as shown in Fig. 9. In the case of the normal process (Fig. 9a), supporting force and upsetting force had the same value with opposite directions, so their effects canceled each other out. Consequently, aluminum alloy close to the interface was under comparatively stable state and relative slip of the contact surfaces was small. However, when a 15° welding groove was machined on the steel (Fig. 9b), the direction of the supporting force angulated to that of the upsetting force and the direction of their resultant force paralleled the contact surface, which was favorable to the extrusion of aluminum alloy near the interface during the upsetting stage. So, relatively less aluminum alloy was available

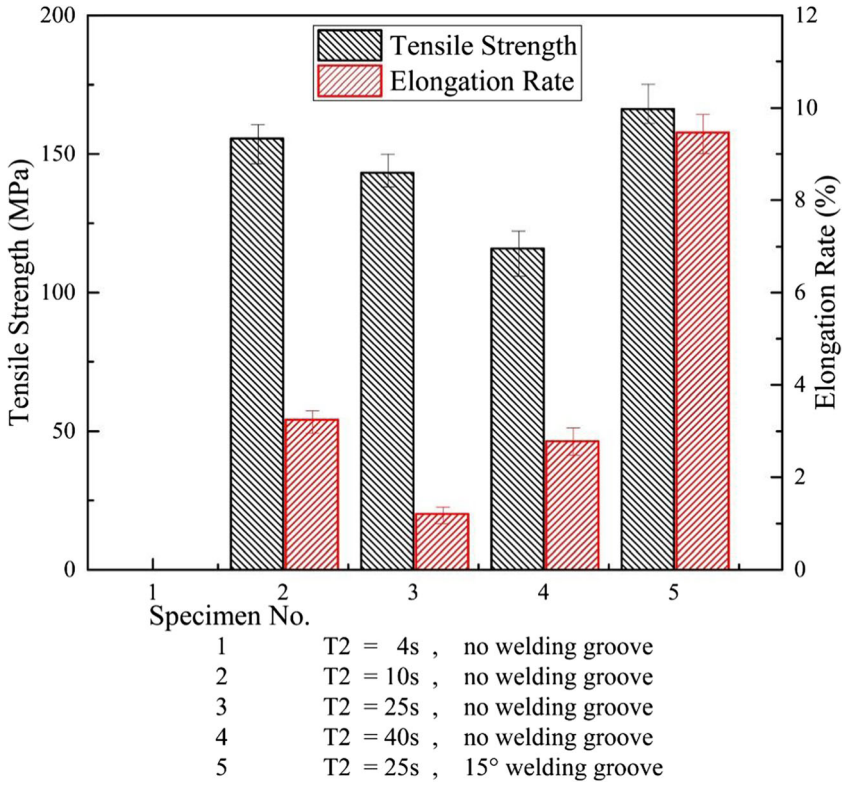

Fig. 12 The comparison of the tensile strength and elongation of specimens 1–5

and the interaction between the metals was restrained, resulting in the thinning of IMC layer.

3.4 Mechanical properties of the joints

Taking specimen 1 for example, the whole range of the aluminum alloy side was investigated by microhardness test, and the result is given in Fig. 10a. The microhardness equal to that of base metal was attained at a place 21 mm far from the interface, which indicated that the width of HAZ in specimen 1 was close to 21 mm and as friction time increased, HAZ would broaden and exceed 21 mm. Figure 10b shows curves of microhardness distribution from a range within an 8-mm distance from the interface on the aluminum alloy side. All the curves showed that after friction welding, hardness of aluminum alloy side declined. This phenomenon was due to the retrogression effect. If precipitation-hardened aluminum alloy was heated to a high temperature under solid solution temperature for a short period, its strength and hardness would decrease, while the elongation and contraction ratio of section increased, such a phenomenon was known as retrogression [32]. In this study, the retrogression temperature of Al–Mg–Si alloy was about 316~540 °C. During the friction welding process, heat generated from the rubbing action between the metals spread from the joint interface to the base metal. The results of temperature measurements when T_2 was 40 s are shown in Fig. 11. Temperature decreased as the distance from the interface increased, so retrogression was less obvious far from the interface. This statement coincided with the upward trend of where was furthest from the interface. And, retrogression effect in specimen 4 was most severe, as hardness declined to the lowest level because of the highest heat input.

It is worth mentioning that during the upsetting stage, if temperature exceeded recrystallization temperature, dynamic recrystallization would occur; however, if not, deformation only triggered work hardening over the process. With regard to specimen 1 ($T_2 = 4$ s), in the absence of solid solution and recrystallization, work hardening played a dominant role over the process. Hardness at and near the interface reached a value of 90.3 HV, which illustrated severe work hardening. However, the hardness declined as the distance from the interface increased, which demonstrates that the effect of work hardening faded gradually. Combined with the optical image shown in Fig. 5c, microhardness of the partial recrystallization zone within specimen 3 was lower than that of the adjacent plastic deformation zone. This phenomenon illustrated that a boundary separated these two regions, and recrystallization occurred on the side near the interface, while work hardening far from the interface. Meanwhile, hardness of the plastic deformation zone within specimen 4 ($T_2 = 40$ s) did not show a sharp rise due to the fact that recrystallization played a dominant role in this situation. The minimum microhardness of specimens 1, 2, and 3 reached 61.8, 61.4, and 57.3 HV at a distance of 6, 3.9, and 2.9 mm from the interface, respectively, which demonstrated that the width of the force-affected zone declined as the friction time increased, as shown in Fig. 10. In

the case of specimen 4 ($T_2 = 40$ s), the deformation generally initiated recrystallization in the joint; thus, the force-affected zone within specimen 4 was narrower.

Friction time and welding groove affect the growth of IMC layers greatly, and the width of IMC layers has a great effect on mechanical properties of the joints, as shown in Fig. 12. Tensile strength of specimen 1 ($T_2 = 4$ s) could be ignored, because it was too low to measure. This was predictable because the bonding between the metals was insufficient under this condition. However, as friction time increased within a certain range, tensile strength of the joints decreased. The heat input rose with increasing friction time; thus, IMC layers at the interface were broadened, leading to the increase of tensile strength. When the secondary friction time $T_2 = 10$ s, the maximum tensile strength of 155.62 MPa was available. On the basis of Fig. 6b, the results suggested that the thickness of IMC layers at the interface of the joint attained under the optimized parameters should be 0.2 μm. However, when the friction time was less than a critical value, tensile strength would decrease sharply due to the incomplete interfacial reaction between the metals involved caused by insufficient heat input. The emergence of non-coalescence cracks at the interface (Fig. 6a) accords with this result.

The fracture surface of specimen 4 ($T_2 = 40$ s) was shown in Fig. 13. A few aluminum alloy was observed to adhere to the steel, and the aluminum alloy side presented a dimple feature, which demonstrated the occurrence of ductile fracture. Meanwhile, the elongation rate of specimen 4 reached 2.78%, which was higher than that of specimen 3. This kind of phenomenon illustrated that exorbitant heat input resulted in lower strength yet higher toughness of the aluminum alloy near the weld, which agreed with the occurrence of the partial secondary recrystallization zone and recrystallization zone with low strength, low hardness, and high plasticity. Besides, welding groove also had a significance effect on mechanical performances. The tensile strength of specimen 5, fabricated with a 15° welding groove on the steel side, was 166.3 MPa, which was 16.15% higher than that of specimen 3 without welding groove. Moreover, it is worth mentioning that the average elongation rate of specimen 5 was

Specimen No.	Secondary Friction Time(s)	Welding Groove	Fracture Location & Morphology
1	4	0	Interface/Plain
2	10	0	Interface/Plain
3	25	0	Interface/Plain
4	40	0	Interface/Ductile [a]
5	25	15°	Al Alloy Side/Ductile

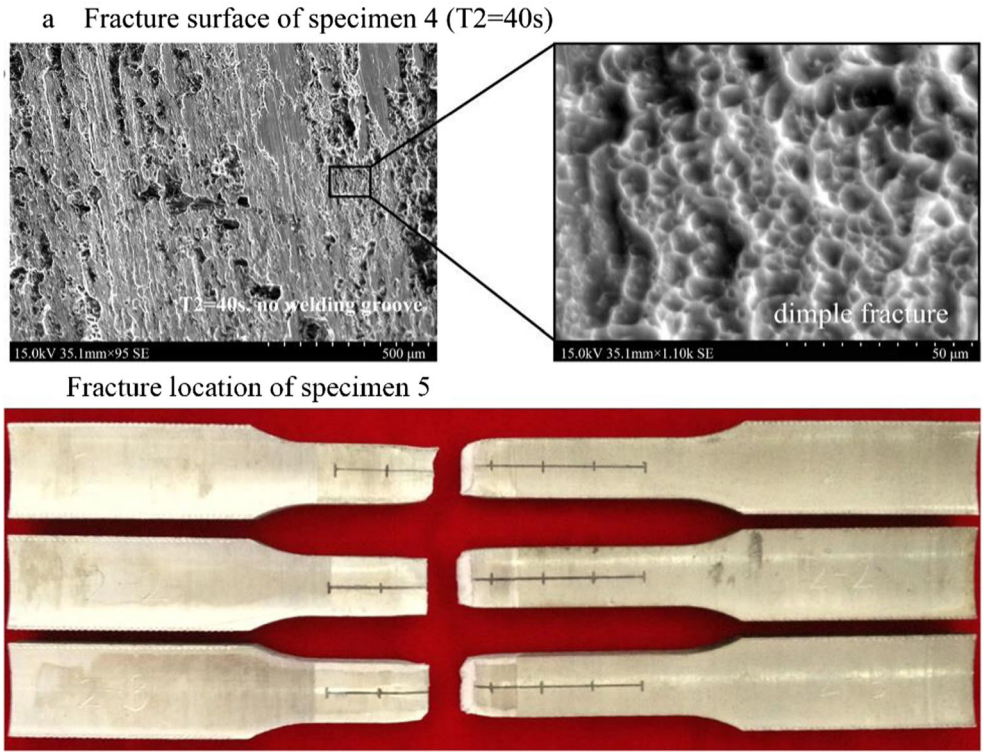

Fig. 13 The fracture surface and fracture location of the specimens after tensile tests

9.47%, which was almost ninth times as large as 1.12% of specimen 3. And, the fracture mode transformed from failure at the interface (specimen 3) into ductile fracture on the aluminum alloy base metal (specimen 5), which indicated that thinning of the IMC layers and expansion of the bonding area brought about by the welding groove had an advantageous effect on the joint strength.

4 Conclusions

Improved friction welding has been applied to join AA6061 alloy and AISI 316L steel successfully with the help of a specific steel collar. The welding processes with different friction time periods were investigated by microstructural analyses and mechanical tests. A 15° welding groove was designed on the steel side to help control the growth of IMC layers. The results are as follows:

1. The most comprehensive region characteristics of the joints consisted of eight different zones. With friction time decreasing, some certain zones were observed to disappear.
2. The thickness of IMC layers increased with elevated friction time. However, the 15° welding groove machined on the steel side contributed to the thinning of the IMC layer with a value of 0.3 μm.
3. Hardness of aluminum alloy side declined compared to that of the base metal due to the retrogression effect. The tensile strength reached 166.32 MPa in the case of processing a 15° welding groove, which was 16.15% higher than that of joint without welding groove. Moreover, the average elongation rate of the joint with welding groove was 9.47%, which was almost ninth times of normal joint.

Funding information The work was jointly supported by the National Natural Science Foundation of China (No. 51575132).

References

1. Torkamany MJ, Tahamtan S, Sabbaghzadeh J (2010) Dissimilar welding of carbon steel to 5754 aluminum alloy by Nd:YAG pulsed laser. Mater Des 31(1):458–465. https://doi.org/10.1016/j.matdes.2009.05.046
2. Zhang Y, Huang J, Cheng Z, Zheng Y, Hai C, Li P, Chen SH (2016) Study on MIG-TIG double-sided arc welding-brazing of aluminum and stainless steel. Mater Lett 172:146–148. https://doi.org/10.1016/j.matlet.2016.02.146
3. Fujii HT, Goto Y, Sato YS, Kokawa H (2016) Microstructure and lap shear strength of the weld interface in ultrasonic welding of Al alloy to stainless steel. Scr Mater 116:135–138. https://doi.org/10.1016/j.scriptamat.2016.02.004
4. Zhang H, Liu J (2011) Microstructure characteristics and mechanical property of aluminum alloy/stainless steel lap joints fabricated by MIG welding-brazing process. Mater Sci Eng A 528(19-20):6179–6185. https://doi.org/10.1016/j.msea.2011.04.039
5. Lin SB, Song JL, Yang CL, Fan CL, Zhang DW (2010) Brazability of dissimilar metals tungsten inert gas butt welding-brazing between aluminum alloy and stainless steel with Al–Cu filler metal. Mater Des 31(5):2637–2642. https://doi.org/10.1016/j.matdes.2009.12.005
6. Zhang MJ, Chen GY, Zhang Y, KR W (2013) Research on microstructure and mechanical properties of laser keyhole welding–brazing of automotive galvanized steel to aluminum alloy. Mater Des 45:24–30. https://doi.org/10.1016/j.matdes.2012.09.023
7. Sierraa G, Peyreb P, Deschaux-Beaumec F, Stuartb D, Frasc G (2007) Steel to aluminium key-hole laser welding. Mater Sci Eng A 447(1-2):197–208. https://doi.org/10.1016/j.msea.2006.10.106
8. Tricarico L, Spina R (2010) Experimental investigation of laser beam welding of explosion-welded steel/aluminum structural transition joints. Mater Des 31(4):1981–1992. https://doi.org/10.1016/j.matdes.2009.10.032
9. Naimon ER, Doyle JH, Rice CR, Walmsley DR (1981) Diffusion welding of aluminum to stainless steel. Weld J 60:17–20
10. Qiu R, Iwamoto C, Satonaka S (2009) Interfacial microstructure and strength of steel/Al alloy joints welded by resistance spot welding with cover plate. J Mater Process Technol 209(8):4186–4193. https://doi.org/10.1016/j.jmatprotec.2008.11.003
11. Lee KJ, Kumai S, Arai T, Aizawac T (2007) Interfacial microstructure and strength of steel/aluminum alloy lap joint fabricated by magnetic pressure seam welding. Mater Sci Eng A 471(1-2):95–101. https://doi.org/10.1016/j.msea.2007.04.033
12. Kore SD, Date PP, Kulkarni SV (2008) Electromagnetic impact welding of aluminum to stainless steel sheets. J Mater Process Technol 208(1-3):486–493. https://doi.org/10.1016/j.jmatprotec.2008.01.039
13. Tsujino J, Hidai K, Hasegawa A, Kanai R, Matsuura H, Matsushima K, Ueoka T (2002) Ultrasonic butt welding of aluminum, aluminum alloy and stainless steel plate specimens. Ultrasonics 40(1-8):371–374. https://doi.org/10.1016/S0041-624X(02)00124-5
14. Coelho RS, Kostka A, Santos JFD, Kaysser-Pyzalla A (2012) Friction-stir dissimilar welding of aluminium alloy to high strength steels: mechanical properties and their relation to microstructure. Mater Sci Eng A 556:175–183. https://doi.org/10.1016/j.msea.2012.06.076
15. Rest CVD, Jacques PJ, Simar A (2014) On the joining of steel and aluminium by means of a new friction melt bonding process. Scr Mater 77:25–28. https://doi.org/10.1016/j.scriptamat.2014.01.008
16. Das H, Ghosh RN, Pal TK (2014) Study on the formation and characterization of the intermetallics in friction stir welding of aluminum alloy to coated steel sheet lap joint. Metal Mater Trans A 45(11):5098–5106. https://doi.org/10.1007/s11661-014-2424-9
17. Lan SH, Liu X, Ni J (2016) Microstructural evolution during friction stir welding of dissimilar aluminum alloy to advanced high-strength steel. Int J Adv Manuf Technol 82(9-12):2183–2193. https://doi.org/10.1007/s00170-015-7531-2
18. Yazdipour A, Heidarzadeh A (2016) Dissimilar butt friction stir welding of Al 5083-H321 and 316L stainless steel alloys. Int J Adv Manuf Technol 87(9-12):3105–3112. https://doi.org/10.1007/s00170-016-8705-2
19. Li W, Vairis A, Preuss M, Ma TJ (2016) Linear and rotary friction welding review. Int Mater Rev 61(2):71–100. https://doi.org/10.1080/09506608.2015.1109214
20. Balalan Z, Ozdemir N, Firat EH, Caligulu U (2015) Functional ANOVA investigation of the effects of friction welding parameters on the joint characteristics of aluminum based MMC to AISI 304 stainless steel. Mater Test 57:558–566
21. Uday MB, Fauzi MNA, Zuhailawati H, Ismail AB (2013) Advances in friction welding process: a review. Sci Technol Weld Join 15:534–558

22. Yılmaz M, Çöl M, Acet M (2002) Interface properties of aluminum/steel friction-welded components. Mater Charact 49(5):421–429. https://doi.org/10.1016/S1044-5803(03)00051-2
23. Kawai G, Ogawa K, Ochi H, Tokisue H (2000) Friction weldability of aluminium alloys to carbon steel. Weld Int 14(2):101–107. https://doi.org/10.1080/09507110009549147
24. Kimura M, Kusaka M, Kaizu K, Nakata K, Nagatsuka K (2015) Friction welding technique and joint properties of thin-walled pipe friction-welded joint between type 6063 aluminum alloy and AISI 304 austenitic stainless steel. Int J Adv Manuf Technol 82:1–11
25. Lee WB, Yeon YM, Kim DU, Jung SB (2003) Effect of friction welding parameters on mechanical and metallurgical properties of aluminium alloy 5052-A36 steel joint. Mater Sci Technol 19(6): 773–778. https://doi.org/10.1179/026708303225001876
26. Fuji A (2004) Friction welding of Al-Mg-Si alloy to Ni-Cr-Mo low alloy steel. Sci Technol Weld Join 9:83–89
27. Fukumoto S, Tsubakino H, Okita K, Aritoshi M, Tomita T (2000) Static joint strength of friction welded joint between aluminium alloys and stainless steel. Weld Int 14(2):89–93. https://doi.org/10.1080/09507110009549145
28. Ikeuchi EK, Makahashi TE, Watanabe MH, Aritoshi M (2009) Effects of carbon content on intermetallic compound layer and joint strength in friction welding of Al alloy to steel. Weld World 53: 135–139
29. Reddy M, Rao S, Mohandas T (2008) Role of electroplated interlayer in continuous drive friction welding of AA6061 to AISI 304 dissimilar metals. Sci Technol Weld Join 13(7):619–628. https://doi.org/10.1179/174329308X319217
30. Elangovan K, Balasubramanian V (2008) Influences of post-weld heat treatment on tensile properties of friction stir-welded AA6061 aluminum alloy joints. Mater Charact 59(9):1168–1177. https://doi.org/10.1016/j.matchar.2007.09.006
31. Fukumoto S, Tsubakino H, Okita K, Tomita T (2013) Friction welding process of 5052 aluminium alloy to 304 stainless steel. Mater Sci Technol 15:1080–1086
32. Reda Y, Abdel-Karim R, Elmahallawi I (2008) Improvements in mechanical and stress corrosion cracking properties in Al-alloy 7075 via retrogression and reaging. Mater Sci Eng A 485(1-2): 468–475. https://doi.org/10.1016/j.msea.2007.08.025